London Journal of PHYSICS

Volume 1 No 2

Characterisation Analysis of Sulphur and Phosphorus Doped and Co-Doped Graphitic Carbon Nitride (g-C_3N_4) Materials

Saba Abbas[1], **Hafsa Khurshid**[2], **Muhammad Irfan**[1], **Muhammad Aamir**[2]

[1]Department of Physics, Mirpur University of Science and Technology (MUST), Mirpur, 10250 AJK, Pakistan.
[2]Department of Chemistry, Mirpur University of Science and Technology (MUST), Mirpur, 10250 AJK, Pakistan.

sabaabbas096@gmail.com

September 25, 2024

Abstract

Graphitic carbon nitride (g-C_3N_4) is tailored with doping of different non-metals (Sulphur and Phosphorus). For synthesis through thermal condensation method, the mixtures of urea and dopant with diverse concentrations have been added for preparation of materials. The basic effect of doping and its concentration on the structural morphology and absorption spectra of the samples is investigated in detail. Pure g-C_3N_4 suffers from high recombination rate of photogenerated electron-hole pairs resulting in low photocatalytic activity. Different techniques like X-ray diffraction (XRD), Scanning electron microscopy (SEM), Fourier transforms infrared (FTIR) spectroscopy, and Photoluminescence spectroscopy (PL) have been used for the characterization. X-ray diffraction studies confirm the formation of the g-C_3N_4 structure and SEM images reveal crumpled sheets and irregular plate like shapes of the doped graphitic nitride samples. FTIR analysis identify the presence of surface amino (N-H) and water (O-H) groups, cyano terminal group (C≡N), (C≡C), (C–N) and (C=N) bonds and breathing mode of the tris-triazine units in the samples. PL spectra shows that the sulphur and phosphorus co-doped PSGCN (8 wt.%) sample is better for photocatalytic activity.

1 Introduction

Graphitic carbon nitride (g-C_3N_4) is a two dimensional (2-D) polymeric semiconductor. It consists of carbon, nitrogen, and some impurity hydrogen [1]. In the presence of visible light, it has commendable stability under ambient conditions and considered as the most encouraging material for the catalysis [2]. It is an inexpensive, narrow bandgap (2.7 eV), metal-free and environmental-friendly material [3]. It contains a group of C-N bond in the π-state without electron localization and it is the most stable allotrope [4, 5]. Carbon nitride (C_3N_4) has wide-ranging family of carbon and nitrogen containing materials, with some impurity hydrogen atoms[6]. The general formula $(C_3N_3H)_n$ is the oldest polymeric material [7].

History of research works on dates back to the 19th century. In 1834, the synthesis of carbon nitride (C3N4) was done by Berzelius and due to its color, it was given the name of as melon by Liebig [8]. Franklin first time recognized its structure as carbon nitride (C_3N_4) in 1922 [9]. Teter and Hemley, in 1996, predicted numerous forms of carbon nitride like α-C_3N_4, cubic-C_3N_4, β-C_3N_4, and pseudo-C_3N_4 [10]. In 1989 it was established that the replacement of Si with Carbon in Silicon Nitride may yield very strong form β-C_3N_4 carbon nitride [11]. Graphitic carbon nitride is a potential candidate for photocatalytic activities in the visible region specially for removing environmental pollutants [12, 13]. Its photocatalytic efficiency has been enhanced by doping with transition, rare earth, alkali and noble metals. Bandgap tailoring of g-C3N4 for enhanced performance has been achieved by Potassium [14] and Sodium [15] doping. Iron, Zirconium, Europium and Cerium doping have improved the photocatalytic ability of g-C_3N_4, due to better absorption of visible

 DOI 10.69710/ljp.v1i2.10365

light.[16] Ag doping of g-C_3N_4 has enhanced the photocatalytic activity seven times due to the utilization of visible light. The Ag_2CO_3/PSGCN was synthesized successfully and utilized as photocatalyst for removal of pollutants from water through electron-hole pair generation [17]. The phosphorous and sulphur co-doping was responsible for narrowing the bandgap to enhance its photodegradation ability under visible light and water remediation [18]. GCN-ZnO composite has shown 3 times better photocatalytic capability as compare to pure GCN, for degradation of water pollutants and methylene blue (MB) dye [13, 19.] The three dimensional Nb_2O_5/ g-C_3N_4 heterostructures have lower bandgap, improved surface area, low carrier recombination rate and improved visible light absorption and remarkable photocatalytic activity [20].

The optical and electrical properties in thermal condensation process depend upon heating rate, precursor type, thermal treatment temperature, duration, and the environment.[21] For the synthesis of g-C_3N_4 high nitrogen content precursors like melamine [22] ($C_3H_6N_6$) cyanamide (CH2N2), dicyandiamide ($C_2H_4N_4$), urea (CH_4N_2O), and thiourea (CH_4N_2S) at higher temperatures (commonly > 550 C) are commonly used. These are bulk materials with small surface area [23]. Among these, the most efficient material is urea for the preparation of g-C_3N_4 which is helpful in producing samples with enhanced surface area, better morphology, improved photocatalytic activity and high physicochemical stability [24].

Thermal condensation of nitrogen-rich precursors such as urea, cyanamide, dicyanamide, melamine, thiourea, trithiocyanuric acid, guanidine hydrochloride, etc. has been the most attractive method for preparation of g-C_3N_4 due its simplicity and use of cheap, readily available precursor [25]. The transformation of the nitrogen-rich precursors to g-C_3N_4 has been proposed starting from cyanamide which condenses to dicyanamide then melamine. This is followed by loss of ammonia and polycondensation to form melamine which is transformed into melamine after loss of ammonia. Further polycondensation yields the polymeric melon, which undergoes rearrangement and polycondensation to yield g-C_3N_4 [26]. The g-C_3N_4 hybridized with graphene oxide (g-C_3N_4/GO) via a sonochemical route showed improved photocatalytic properties of degradation under visible light exposure.[27] It was observed that the ternary nanostructure was significantly more photocatalytic active compared to g-C_3N_4 [28]. The g-C_3N_4@TiO2 core-shell structure photocatalysts with controlled ultra-thin g-C_3N_4 layers were prepared by a new method of the sol-gel approaches in situ coating re-assembled. It strong binding force between the core and shell, which is stable, without secondary pollution and convenient for recovery [29].

Tremendous interest in graphitic carbon nitride as a photocatalyst has seen it emerging as fascinating materials in various scientific fields such as environmental pollution abatement, hydrogen evolution from water splitting, solar cells, sensors, energy storage, etc. [30]. These applications exploit some of the fascinating properties of g-C_3N_4 which include visible light response, good oxidation power, environmental friendliness, good chemical and thermal stability, metal-free nature, easy fabrication from readily available precursors and its polymeric structure allows for easy modifications to alter its properties [31]. Such nanostructures include metal and non-metal doped g-C_3N_4, g-C_3N_4/carbon nanomaterials heterojunctions, binary and ternary nanocomposites32. The charge transfer mechanisms involved in the various heterostructures have been discussed in detail 33. Improved visible light photocatalytic performance has been observed upon formation of the various heterostructures and this has been credited to improved specific surface area, efficient charge separation and transfer, improved generation. Graphitic carbon nitride (g-C_3N_4), a polymeric, metal-free semiconductor has become hot-spot in various scientific exploits such as environmental pollution mitigation, energy generation and storage, organic synthesis, sensors, etc. [5, 34]

2 Experimental Methods

Several methods have been explored for the preparation of g-C_3N_4 with different architectures and electronic properties. Such methods include chemical vapour deposition (CVD), solvothermal, physical vapour deposition (PVD), ionothermal synthesis, solid state, sonochemical and thermal condensation methods. We have used thermal condensation method for the preparation of sulphur and phosphorus doped g-C_3N_4 samples. The diammonium hydrogen phosphate was used as phosphorus source during PGCN synthesis. It depends upon heating rate, precursor type, thermal treatment temperature, duration, and environment. The easiest method to make g-C_3N_4 includes high nitrogen content precursors like melamine ($C_3H_6N_6$), cyanamide (CH_2N_2), dicyandiamide ($C_2H_4N_4$), urea (CH_4N_2O), and thiourea (CH_4N_2S) at higher temperatures (commonly > 550C).

 DOI 10.69710/ljp.v1i2.10365

2.1 Samples

The samples are prepared by thermal condensation method. Urea, diammonium hydrogen phosphate and thiourea are used as precursors of g-C_3N_4, PGCN, SGCN and PSGCN.

2.2 Preparation of g-C_3N_4

In this preparation of samples 5 g of urea was mixed with 8 wt.% of diammonium hydrogen phosphate and thiourea. Added 10 ml of distilled water and stirred it for 2 hours. After stirring the solution then start heated at 90 oC for 1.5 hours. After cooling, the material was crushed and annealed in closed ceramic crucible at 550 ˚C for 4 hours at heating rate 10 ˚C/mint. The final product was in the form of powder. Similarly, the samples with 16 wt.% and 32 wt.% doping were prepared by the same method.

3 Results and Discussions

3.1 X-RAY DIFFRACTION ANALYSIS

X-ray spectra of GCN, PGCN, SGCN, and PSGCN show three prominent peaks (100), (002) and (101). The (100) plane is attributed to the in-plane tri-s-triazine nitrogen linkage motifs and (002) plane shows the periodic stacking layers of conjugated aromatic rings 35. The (101) plane is the confirmation of amorphous structure of g-C_3N_4 [36].

The XRD patterns of pure g-C_3N_4, phosphorus doped, and then phosphorus and sulphur co-doped g-C_3N_4 (8 wt.%) samples are given in Fig. 1(a). As a result interplanar stacking distance (d) has decreased to improve polymerization and dense packing in phosphorus doped g-C_3N_4.

Table 1: Interplanar distances and hkl values of (8 wt %) samples.

Samples	**hkl**	**2 Θ (°)**	**d (Å)**
GCN	(100)	17.29	5.125
PGCN-8%	(100)	18.36	4.8125
PSGCN-8%	(100)	17.57	5.04
GCN	(002)	29.47	3.029
PGCN-8%	(002)	29.81	2.99
PSGCN-8%	(002)	28.90	3.095
GCN	(101)	40.41	2.23
PGCN-8%	(101)	39.16	2.295
PSGCN-8%	(101)	38.14	2.355

Table 1. shows interplanar distances for (8 wt.%) (002) the value of d has decreased for PGCN and increased for PSGCN. While for (101) it has increased in both the samples.

XRD patterns of pure g-C_3N_4 with 16 wt % doping are shown in Fig. 1(b). Table 2. shows that after doping the interplanar distance d has decreased for (001) peak. For (002) the value of d has decreased PGCN and SGCCN and increased for PSGCN. While for (101) the value of d has increased PGCN and PSGCN, but reduced in SGCN. As a result interplanar stacking distance (d) has decreased to improve polymerization and dense packing in phosphorus doped g-C_3N_4 [37].

Table 2: Interplanar distance and hkl values of (16 wt.%) samples.

 DOI 10.69710/ljp.v1i2.10365

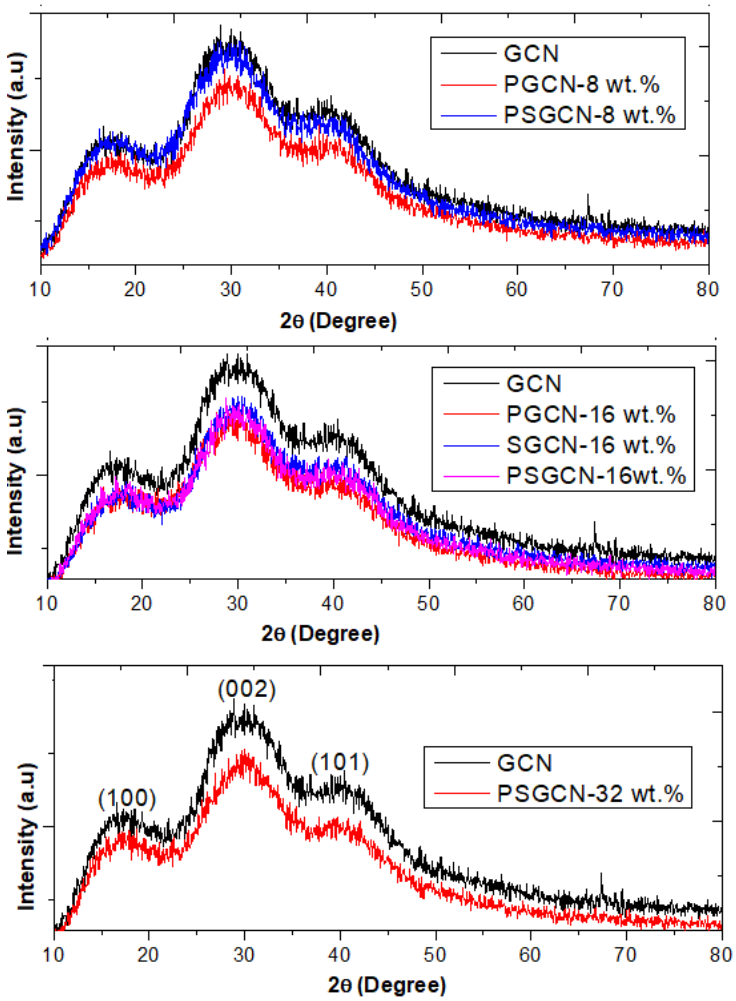

Figure 1: XRD Graphs of all percentages ((a) 8 wt.%, (b) 16 wt.%, and (c) 32 wt.

Samples	**hkl**	**2Θ (°)**	**d (Å)**
GCN	(100)	17.29	5.125
PGCN-16%	(100)	17.46	5.075
SGCN-16%	(100)	18.25	4.86
PSGCN-16%	(100)	17.34	5.11
GCN	(002)	29.47	3.029
PGCN-16%	(002)	30.38	2.94
SGCN-16%	(002)	31.40	2.845
PSGCN-16%	(002)	28.79	3.095
GCN	(101)	40.41	2.23
PGCN-16%	(101)	39.44	2.28
SGCN-16%	(101)	41.32	2.18
PSGCN-16%	(101)	39.45	2.28

XRD patterns of pure g-C_3N_4 with 32 wt.% doping are shown in Fig. 1(c). (100) peak has shown hole-to-hole distance corresponding to the nitride pores and (002) peak measure distance between the stacked layers of aromatic units. As a result interplanar stacking distance (d) has decreased to improve polymerization and dense packing in phosphorus doped g-C_3N_4. The (101) peak shows the amorphous carbon structure in

 DOI 10.69710/ljp.v1i2.10365

the samples. In Table.3, we observe that interplanar spacing d for (001) and (002) diffraction peaks have reduced, on the other hand has increased for (101) plane.[38]

Table 3: Interplanar distance and hkl values of (32 wt.%) samples.

Samples	**hkl**	**2Θ (°)**	**d (Å)**
GCN	(100)	17.29	5.125
PSGCN-32%	(100)	18.70	4.74
GCN	(002)	29.47	3.029
PSGCN-32%	(002)	30.04	2.94
GCN	(101)	40.41	2.23
PSGCN-32%	(101)	39.78	2.26

3.2 SCANNING ELECTRON MICROSCOPY (SEM)

Scanning electron microscopy has been employed to examine morphology of un-doped, sulphur doped, and sulphur-phosphorous co-doped graphitic carbon nitrides (g-C_3N_4, SGCN, and PSGCN) samples.

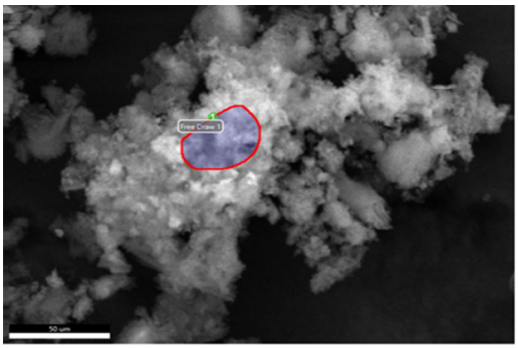

Figure 2: SEM image of g-C_3N_4 Sample.

In as prepared un-doped GCN sample the SEM image (Fig. 2), shows irregular, non-smooth irregular plate type structure, this has been shown in the enlarged image.

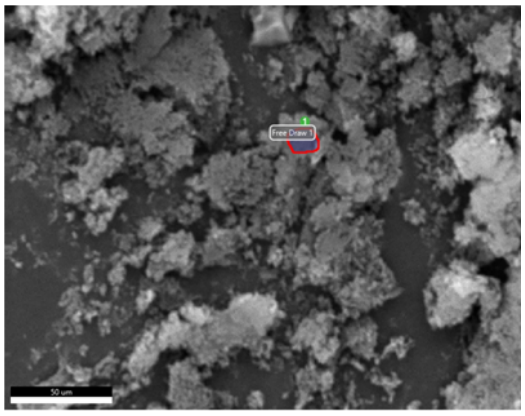

Figure 3: SEM image of SGCN Sample.

The SGCN image represent sulphur doped sample is shown in Fig.3, shows crumpled sheets, irregular flakes due to decreased interplanar distance as seen from X-ray diffractogram. The layered structure decom-

 DOI 10.69710/ljp.v1i2.10365

posed due to presence of sulphur in GCN indicating that doping had reduced crystal growth of GCN. This disordered structure of SGCN is most likely caused by higher atomic radius of the sulphur.[39]

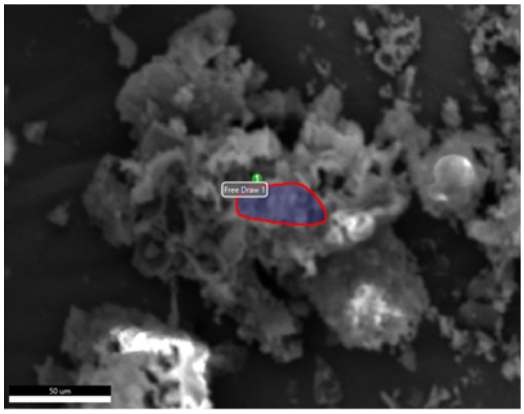

Figure 4: SEM image of PSGCN Sample.

Fig. 4 shows laminar large sized sheet like structure for co-doped PSGCN samples, because of increased interplanar distance as seen from the XRD. The flakes irregular with some agglomeration.

3.3 FOURIER TRANSFORM INFRARED SPECTROSCOPY (FTIR)

FTIR graphs, in the range 500-3500 cm^{-1}, of un-doped g-C_3N_4, PGCN and SGCN and PSGCN are displayed in Fig. 5. The range 500-1500 cm^{-1} represents fingerprint region of skeletal vibrations, 1500-2000 cm^{-1} show double bonds, 2000-2500 cm^{-1} indicates triple bonds and 2500-3500 cm-1 single bond between the atoms.

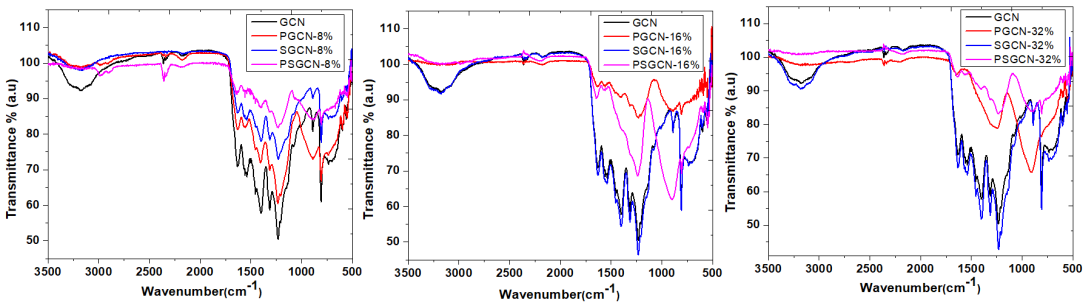

Figure 5: Combined FTIR Graph of all percentages (8, 16, and 32 wt.%.

Fig.5 shows that strong evidence of the formation of desired structure is the presence of characteristic bending mode of the tri-s-triazine units around at 800 cm^{-1}. In PSGCN (8 wt.%) it shifted from 808 to 800 cm^{-1}, but it remains unchanged in sulphur doped specimen. In PGCN and PSGCN (16 wt.%) intensity has decreased and is shifted from 808 to 802, and 806 cm-1, but it remains unchanged in sulphur doped specimen. In SGCN and PSGCN (32 wt.%) intensity has decreased and is shifted from 808 cm-1 to 804 cm-1, but it increased in phosphorus doped specimen. The FTIR spectra have confirmed the formation of a g-C_3N_4 phase in all samples as it contains skeletal vibrational modes of C-N heterocycles in the 1200-1700 cm^{-1} region. The band is clearly visible in all specimens, but peak intensity is decreasing with doping and co-doping which can be attributed to the changes in the structure.[40] For the carbon dioxide related bond (C≡C) the wavenumber has reduced and shifted to 2165-2195 cm^{-1} for PGCN, SGCN and PSGCN samples, respectively. Another vibrational mode corresponding to vibrating cyano terminal group (C≡N) is appearing at 2355-2365 cm^{-1} for g-C_3N_4, SGCN, PGCN, and PSGCN samples. The intensity of this mode has enhanced with the doping and co doping. FTIR spectrum of GCN, PGCN, SGCN, and PSGCN show broad bands of stretching and

 DOI 10.69710/ljp.v1i2.10365

deformation modes of -NH2 groups at 3180-3130cm^{-1} respectively, with decreased intensity in all samples [41].

3.4 PHOTOLUMINESCENCE SPECTROSCOPY

The optical properties of different samples were studied by the Photoluminescence (PL) spectra analysis. PL spectra reflect the charge transfer, capture and recombination of electron-hole pairs of photocatalytic material. The high-strength photocatalytic material has a large amount of photogenerated carriers and good photocatalytic performance. Conversely, the photocatalytic material with low strength has less photogenerated carriers and poor photocatalytic performance [42].

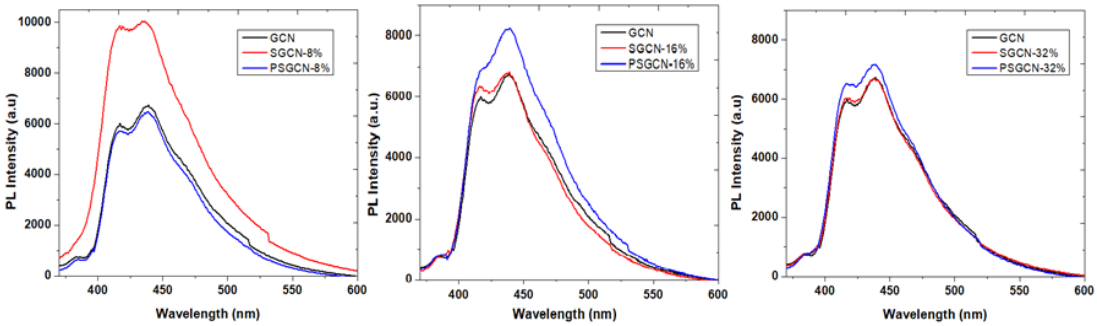

Figure 6: Combined PL spectra of all percentages (8, 16, and 32 wt. %.)

The photoluminescence spectra of un-doped g-C_3N_4, SGCN and PSGCN samples are displayed in Fig. 6. All samples show broad intense luminescence peaks in the 400-450 nm range. This emission peak can be ascribed to the radioactive recombination of electron-hole pairs. Combined spectra (8 wt.%) show that slight blue shifting has been observed after doping and co-doping. Intensity of sulphur doped sample has enhanced significantly but it has decreased marginally in sulphur-phosphorous co-doped sample. It means the co-doped PSGCN (8 wt.%) sample is slightly better for photocatalytic activity. For 16 wt.% and 32 wt.%, shows that no considerable shift in peak positions, and reveals increased intensity in the co-doped material which is attributed to higher electron hole recombination rate. It gives new results which means negative impact on photocatalytic activities of the samples which is contradictory to the reported results. On the other hand, the sulphur doped sample has shown no considerable variation both in peak position and intensity.

4 CONCLUSIONS

To prepare the pure g-C_3N_4, Phosphorus and Sulphur doped and co-doped g-C_3N_4 samples by thermal condensation method. The structural and optical properties were measured by XRD, SEM, FTIR, and PL spectroscopy analysis. X-ray diffraction peaks (100), (002) and (101) have been observed in all samples which represent hexagonal phase. Presence of these peaks confirmed that the structure of g-C_3N_4 has been retained after doping and co-doping with Sulphur and Phosphorus. The SGCN SEM image sample shows crumpled sheets, irregular flakes due to decreased interplanar distance in accordance with the X-ray diffraction result. The laminar large sized sheet like structure is observed in SEM image of co-doped sample. The morphology of PS- g-C_3N_4 sample reveals irregular flakes, and agglomerates with sizes up to 50 µm. In FTIR spectra, show that strong evidence of the formation of desired structure is the presence of characteristic breathing mode of the tri-s-triazine units around at 800 cm^{-1}. The typical skeletal vibrations of aromatic C-N heterocycles appearing at 1200-1700 cm-1 are related to (C–N) and (C=N) bonds and confirm the formation of g-C_3N_4 phase. For the carbon dioxide related bond (C≡C) the wavenumber has reduced and shifted to 2165-2195 cm^{-1} for PGCN, SGCN and PSGCN samples, respectively. Another vibrational mode corresponding to vibrating cyano terminal group (C≡N) is appearing at 2355-2365 cm^{-1} for g-C_3N_4, SGCN, PGCN, and PSGCN samples. The intensity of this mode has enhanced with the doping and co doping. FTIR spectrum of GCN, PGCN, SGCN, and PSGCN show broad bands of stretching and deformation modes of -NH_2 groups

 DOI 10.69710/ljp.v1i2.10365

at 3180-3130cm^{-1} respectively, with decreased intensity in all samples. PL spectra shows that the Sulphur and Phosphorus co-doped PSGCN (8 wt.%) sample is better for photocatalytic activity.

5 Acknowledgements

I thank my teachers and family for their constant motivation throughout this research endeavor. Special thanks to Muhammad Irfan and Dr. Muhammad Aamir for the necessary guidance and unwavering motivation.

6 Copyright Notice

References

[1] Zhu, J.; Xiao, P.; Li, H.; Carabineiro, S. A. Graphitic carbon nitride: synthesis, properties, and applications in catalysis. ACS applied materials & interfaces 2014, 6 (19), 16449-16465.

[2] Maeda, K.; Wang, X.; Nishihara, Y.; Lu, D.; Antonietti, M.; Domen, K. Photocatalytic activities of graphitic carbon nitride powder for water reduction and oxidation under visible light. The Journal of Physical Chemistry C 2009, 113 (12), 4940-4947. Qin, L.; Huang, D.; Xu, P.; Zeng, G.; Lai, C.; Fu, Y.; Yi, H.; Li, B.; Zhang, C.; Cheng, M. In-situ deposition of gold nanoparticles onto polydopamine-decorated g-C3N4 for highly efficient reduction of nitroaromatics in environmental water purification. Journal of colloid and interface science 2019, 534, 357-369.

[3] Wang, Y.; Liu, L.; Ma, T.; Zhang, Y.; Huang, H. 2D graphitic carbon nitride for energy conversion and storage. Advanced Functional Materials 2021, 31 (34), 2102540.

[4] Mo, R.; Li, J.; Tang, Y.; Li, H.; Zhong, J. Introduction of nitrogen defects into a graphitic carbon nitride framework by selenium vapor treatment for enhanced photocatalytic hydrogen production. Applied Surface Science 2019, 476, 552-559.

[5] Khurshid, H.; Ali, Y.; Saleem, M.; Khurshid, Z.; Aamir, M.; Yasir, M. Recent Advances in MOF-Derived Carbon Materials for Energy Storage: Powering the Future. Journal of Chemistry and Material Sciences (JCMS) 2024, 1 (1), 53-66.

[6] She, X.; Wu, J.; Zhong, J.; Xu, H.; Yang, Y.; Vajtai, R.; Lou, J.; Liu, Y.; Du, D.; Li, H. Oxygenated monolayer carbon nitride for excellent photocatalytic hydrogen evolution and external quantum efficiency. Nano Energy 2016, 27, 138-146. Wang, H.; Sun, Z.; Li, Q.; Tang, Q.; Wu, Z. Surprisingly advanced CO2 photocatalytic conversion over thiourea derived g-C3N4 with water vapor while introducing 200–420 nm UV light. Journal of CO2 Utilization 2016, 14, 143-151.

[7] Ma, Y.; Zhang, J.; Wang, Y.; Chen, Q.; Feng, Z.; Sun, T. Concerted catalytic and photocatalytic degradation of organic pollutants over CuS/g-C3N4 catalysts under light and dark conditions. Journal of advanced research 2019, 16, 135-143.

[8] Liebig, J. Uber einige Stickstoff-Verbindungen. Annalen der Pharmacie 1834, 10 (1), 1-47.

[9] Franklin, E. C. The ammono carbonic acids. Journal of the American Chemical Society 1922, 44 (3), 486-509.

[10] Teter, D. M.; Hemley, R. J. Low-compressibility carbon nitrides. Science 1996, 271 (5245), 53-55.

[11] Idris, A. O.; Oseghe, E. O.; Msagati, T. A.; Kuvarega, A. T.; Feleni, U.; Mamba, B. Graphitic carbon nitride: a highly electroactive nanomaterial for environmental and clinical sensing. Sensors 2020, 20 (20), 5743.

[12] Mehmood, Z.; Khurshid, H.; Khurshid, Z.; Aamir, M.; Khan, M. Enhanced Removal of Dyes from Wastewater through Photocatalysis: Overview and Perspectives.

[13] Khurshid, H.; Mehmood, Z.; Naseer, S.; Aamir, M.; Khurshid, F.; Khan, M. Evaluating the Efficiency of Photocatalytic Degradation in Tetracycline Removal: A Comprehensive Review. PAKISTAN JOURNAL OF BIOCHEMISTRY AND MOLECULAR BIOLOGY 2023, 56 (3), 117-128.

[14] Mamba, G.; Mishra, A. Graphitic carbon nitride (g-C3N4) nanocomposites: a new and exciting generation of visible light driven photocatalysts for environmental pollution remediation. Applied Catalysis B: Environmental 2016, 198, 347-377.

[15] Zhang, M.; Bai, X.; Liu, D.; Wang, J.; Zhu, Y. Enhanced catalytic activity of potassium-doped graphitic carbon nitride induced by lower valence position. Applied Catalysis B: Environmental 2015, 164, 77-81.

[16] Zhou, X.; Peng, F.; Wang, H.; Yu, H.; Fang, Y. Carbon nitride polymer sensitized TiO 2 nanotube arrays with enhanced visible light photoelectrochemical and photocatalytic performance. Chemical Communications 2011, 47 (37), 10323-10325. Hu, S.; Jin, R.; Lu, G.; Liu, D.; Gui, J. The properties and photocatalytic performance comparison of Fe 3+-doped gC 3 N 4 and Fe 2 O 3/gC 3 N 4 composite catalysts. Rsc Advances 2014, 4 (47), 24863-24869.

[17] She, P.; Li, J.; Bao, H.; Xu, X.; Hong, Z. Green synthesis of Ag nanoparticles decorated phosphorus doped g-C3N4 with enhanced visible-light-driven bactericidal activity. Journal of Photochemistry and Photobiology A: Chemistry 2019, 384, 112028.

[18] Pan, T.; Chen, D.; Fang, J.; Wu, K.; Feng, W.; Zhu, X.; Fang, Z. Facile synthesis of iron and cerium co-doped g-C3N4 with synergistic effect to enhance visible-light photocatalytic performance. Materials Research Bulletin 2020, 125, 110812.

[19] Raizada, P.; Sudhaik, A.; Singh, P.; Shandilya, P.; Thakur, P.; Jung, H. Visible light assisted photodegradation of 2, 4-dinitrophenol using Ag2CO3 loaded phosphorus and sulphur co-doped graphitic carbon nitride nanosheets in simulated wastewater. Arabian Journal of Chemistry 2020, 13 (1), 3196-3209.

[20] Paul, D. R.; Gautam, S.; Panchal, P.; Nehra, S. P.; Choudhary, P.; Sharma, A. ZnO-modified g-C3N4: a potential photocatalyst for environmental application. ACS omega 2020, 5 (8), 3828-3838.

[21] Subashini, A.; Prasath, P. V.; Sagadevan, S.; Lett, J. A.; Fatimah, I.; Mohammad, F.; Al-Lohedan, H. A.; Alshahateet, S. F.; Oh, W. C. Enhanced photocatalytic degradation efficiency of graphitic carbon nitride-loaded CeO2 nanoparticles. Chemical Physics Letters 2021, 769, 138441.

[22] Idrees, F.; Dillert, R.; Bahnemann, D.; Butt, F. K.; Tahir, M. In-situ synthesis of Nb2O5/g-C3N4 heterostructures as highly efficient photocatalysts for molecular H2 evolution under solar illumination. Catalysts 2019, 9 (2), 169.

[23] Xing, Y.; Wang, X.; Hao, S.; Zhang, X.; Wang, X.; Ma, W.; Zhao, G.; Xu, X. Recent advances in the improvement of g-C3N4 based photocatalytic materials. Chinese Chemical Letters 2021, 32 (1), 13-20.

[24] Dong, F.; Zhao, Z.; Xiong, T.; Ni, Z.; Zhang, W.; Sun, Y.; Ho, W.-K. In situ construction of g-C3N4/g-C3N4 metal-free heterojunction for enhanced visible-light photocatalysis. ACS applied materials & interfaces 2013, 5 (21), 11392-11401.

[25] Kumar, S.; Surendar, T.; Kumar, B.; Baruah, A.; Shanker, V. Synthesis of highly efficient and recyclable visible-light responsive mesoporous gC 3 N 4 photocatalyst via facile template-free sonochemical route. RSC advances 2014, 4 (16), 8132-8137. Dong, G.; Zhang, Y.; Pan, Q.; Qiu, J. A fantastic graphitic carbon nitride (g-C3N4) material: electronic structure, photocatalytic and photoelectronic properties. Journal of Photochemistry and Photobiology C: Photochemistry Reviews 2014, 20, 33-50.

[26] Abd El-kader, F.; Moharram, M.; Khafagia, M.; Mamdouh, F. Influence of the nitrogen content on the optical properties of CNx films. Spectrochimica Acta Part A: Molecular and Biomolecular Spectroscopy 2012, 97, 1115-1119. Dontsova, D.; Pronkin, S.; Wehle, M.; Chen, Z.; Fettkenhauer, C.; Clavel, G.; Antonietti, M. Triazoles: a new class of precursors for the synthesis of negatively charged carbon nitride derivatives. Chemistry of Materials 2015, 27 (15), 5170-5179.

[27] Tahir, M.; Mahmood, N.; Zhang, X.; Mahmood, T.; Butt, F. K.; Aslam, I.; Tanveer, M.; Idrees, F.; Khalid, S.; Shakir, I. Bifunctional catalysts of Co 3 O 4@ GCN tubular nanostructured (TNS) hybrids for oxygen and hydrogen evolution reactions. Nano Research 2015, 8, 3725-3736.

[28] Liao, G.; Chen, S.; Quan, X.; Yu, H.; Zhao, H. Graphene oxide modified gC 3 N 4 hybrid with enhanced photocatalytic capability under visible light irradiation. Journal of Materials Chemistry 2012, 22 (6), 2721-2726.

[29] Wang, Y.; Yang, W.; Chen, X.; Wang, J.; Zhu, Y. Photocatalytic activity enhancement of core-shell structure g-C3N4@ TiO2 via controlled ultrathin g-C3N4 layer. Applied Catalysis B: Environmental 2018, 220, 337-347.

[30] Wirth, J.; Neumann, R.; Antonietti, M.; Saalfrank, P. Adsorption and photocatalytic splitting of water on graphitic carbon nitride: a combined first principles and semiempirical study. Physical Chemistry Chemical Physics 2014, 16 (30), 15917-15926.

[31] Chang, F.; Xie, Y.; Li, C.; Chen, J.; Luo, J.; Hu, X.; Shen, J. A facile modification of g-C3N4 with enhanced photocatalytic activity for degradation of methylene blue. Applied Surface Science 2013, 280, 967-974. Pany, S.; Parida, K. A facile in situ approach to fabricate N, S-TiO 2/gC 3 N 4 nanocomposite with excellent activity for visible light induced water splitting for hydrogen evolution. Physical Chemistry Chemical Physics 2015, 17 (12), 8070-8077.

[32] Gowri, V. M.; Ajith, A.; John, S. A. Systematic study on morphological, electrochemical impedance, and electrocatalytic activity of graphitic carbon nitride modified on a glassy carbon substrate from sequential exfoliation in water. Langmuir 2021, 37 (35), 10538-10546.

[33] Zhang, H.; Huang, Y.; Hu, S.; Huang, Q.; Wei, C.; Zhang, W.; Yang, W.; Dong, P.; Hao, A. Self-assembly of graphitic carbon nitride nanosheets–carbon nanotube composite for electrochemical simultaneous determination of catechol and hydroquinone. Electrochimica Acta 2015, 176, 28-35.

[34] Zhao, Y.; Tang, R.; Huang, R. Palladium supported on graphitic carbon nitride: an efficient and recyclable heterogeneous catalyst for reduction of nitroarenes and Suzuki coupling reaction. Catalysis Letters 2015, 145, 1961-1971. Yang, Q.; Wang, W.; Zhao, Y.; Zhu, J.; Zhu, Y.; Wang, L. Metal-free mesoporous carbon nitride catalyze the Friedel–Crafts reaction by activation of benzene. RSC Advances 2015, 5 (68), 54978-54984.

[35] Guan, K.; Li, J.; Lei, W.; Wang, H.; Tong, Z.; Jia, Q.; Zhang, H.; Zhang, S. Synthesis of sulfur doped g-C3N4 with enhanced photocatalytic activity in molten salt. Journal of Materiomics 2021, 7 (5), 1131-1142.

[36] Wang, Y.; Wang, X. M. antonietti. ACS Catal 2012, 2, 1596-1606.

[37] Zheng, Y.; Liu, J.; Liang, J.; Jaroniec, M.; Qiao, S. Z. Graphitic carbon nitride materials: controllable synthesis and applications in fuel cells and photocatalysis. Energy & Environmental Science 2012, 5 (5), 6717-6731.

[38] Moussa, H.; Chouchene, B.; Gries, T.; Balan, L.; Mozet, K.; Medjahdi, G.; Schneider, R. Growth of ZnO nanorods on graphitic carbon nitride gCN sheets for the preparation of photocatalysts with high visible-light activity. ChemCatChem 2018, 10 (21), 4973-4983.

[39] Ahmed, A.; Hayat, A.; Nawaz, M. H.; John, P.; Nasir, M. Construction of sponge-like graphitic carbon nitride and silver oxide nanocomposite probe for highly sensitive and selective turn-off fluorometric detection of hydrogen peroxide. Journal of colloid and interface science 2020, 558, 230-241.

[40] Yang, J.-H.; Kim, S.; Kim, I. Y.; Lee, J. M.; Yi, J.; Karakoti, A.; Joseph, S.; Albahily, K.; Vinu, A. Highly enhanced photocatalytic hydrogen evolution activity of graphitic carbon nitride with 3D connected mesoporous structure. Sustainable materials and technologies 2020, 25, e00184.

[41] Ghashghaee, M.; Azizi, Z.; Ghambarian, M. Conductivity tuning of charged triazine and heptazine graphitic carbon nitride (g-C3N4) quantum dots via nonmetal (B, O, S, P) doping: DFT calculations. Journal of Physics and Chemistry of Solids 2020, 141, 109422.

[42] Liu, D.; Dong, J.; Liu, F.; Gao, X.; Yu, Y.; Zhang, S.; Dong, L.; Guo, Y. SYNTHESIS AND PHOTOCATALYTIC PERFORMANCE OF gC 3N4 COMPOSITES. Journal of Ovonic Research Vol 2019, 15 (4), 239-246.

 DOI 10.69710/ljp.v1i2.10365